Polarized neutron reflection as a probe of magnetic films and multilayers

S. J. Blundell and J. A. C. Bland
Cavendish Laboratory, Madingley Road, Cambridge, CB3 0HE, United Kingdom
(Received 16 December 1991)

The application of polarized neutron reflection (PNR) to the study of the magnetic properties of thin films and multilayers is described. It is demonstrated that PNR provides a means of directly determining the magnetization-vector profile in multilayers of known layer thickness and layer density. Thus, the magnetization reversal process in these systems can be directly studied. A matrix method is presented which can be used to calculate the spin-dependent reflectivity from a multilayer with general in-plane orientation of the magnetic moment in each layer. In addition, we show that behavior of the spin asymmetry is dominated by multiple reflections and refraction just above the critical wave vector, but with increasing wave vector, such processes become progressively less important, and the response moves towards a "diffraction limit" in which a Fourier-transform approximation to the exact result can be used. The ideas in this paper are illustrated by a number of examples, including the exchange-biased structure Ag/Fe-Ni/Cu/Fe-Ni/Fe-Mn/Si.

I. INTRODUCTION

The coupling between ultrathin magnetic films has become a subject of strong interest. An antiferromagnetic coupling between two ferromagnetic layers has been observed in Fe/Cr/Fe(001) using Brillouin light scattering[1] and SPLEED.[2] This interaction has been observed to oscillate between ferromagnetic and antiferromagnetic coupling as a function of spacer thickness in Gd/Y superlattices,[3] Co/Cu/Co,[4] and sputtered $(Co/Ru)_n$ and $(Fe/Cr)_n$ superlattices.[5] The length scale of this oscillation is beginning to be understood in terms of the band structure of the spacer layer,[6] although several questions remain, particularly concerning the detailed magnetic structure resulting from the coupling. These couplings are of great interest because of the large magnetoresistance (MR) which is observed in antiferromagnetically coupled systems,[7] although large MR effects are also seen in films between which exchange coupling is weak, as has been demonstrated by recent experiments on Fe-Ni/Cu/Fe-Ni/Fe-Mn.[8] The large MR is interpreted in terms of a "spin-valve" effect[8] in which the relative orientation between the magnetizations in the two layers controls the magnetoresistance. It is therefore of interest to study directly the magnetization reversal processes in such structures.

In this paper we wish to describe and demonstrate the way in which the technique of polarized neutron reflection (PNR) can be used to measure the magnetization-vector profile of a multilayer system of known layer thickness and layer density, in which the magnetizations of individual magnetic layers need not be parallel. It can therefore be used to determine the relative orientation of the magnetizations in a coupled film. PNR has already been used to measure the magnetization of single films (e.g., Co/Cu,[9] and Fe/Ag[10]) and to study the magnetization profile in nanometer thick Co/GaAs[11] and in a coupled Fe/Cr/Fe multilayer.[12] In this latter case, the interpretation is complicated by the fact that multidomain formation occurs. PNR has also been used to show that the magnetization in the ferromagnetic component of an Fe-Ni/Fe-Mn bilayer structure is uniform.[13] Here, we choose to illustrate our discussion of the technique with Fe-Ni/Cu/Fe-Ni/Fe-Mn; this is a convenient model system in which the relative orientation of the Fe-Ni magnetizations can be controlled, and in which the ferromagnetic layers are single domain for appropriate values of applied field.[8] To understand the PNR technique, it is necessary to examine the reflection, refraction, and interference processes that can occur in neutron reflection from these systems. We show that the form of the spin asymmetry is dominated by multiple reflections and refraction just above the critical wave vector, but with increasing wave vector, such processes become progressively less important, and the response moves toward a "diffraction limit" in which a Fourier-transform approximation to the exact result can be used. We begin with a discussion of these processes in simple systems. The theory of neutron reflection from multilayers will be described in Sec. II, and this will be extended to a fully spin-dependent theory in Sec. VI. Examples will be presented in Secs. III–V and VII to illustrate these ideas. The use of the technique in studying single layers has been described previously.[14]

II. NEUTRON REFLECTION

The Schrödinger equation for the wave function of a neutron in a solid $\Psi(\mathbf{r})$, can be written in general as

$$\left[\frac{-\hbar^2}{2m_n}\nabla^2+V(\mathbf{r})\right]\Psi(\mathbf{r})=E\Psi(\mathbf{r})\ , \tag{1}$$

where m_n and $V(\mathbf{r})$ are the neutron mass and potential energy. We will model the sample as a multilayer containing n homogeneous regions numbered so that region 1 is vacuum, region n is substrate, and the evaporated

layers are the regions in between, i.e., $2,3,\ldots,n-1$. We also assume that the multilayer has flat interfaces between these regions and so it possesses translational invariance in the (x,z) plane. We can then write the neutron wave function $\Psi(\mathbf{r})$ in terms of $k_\parallel$, the neutron wave vector parallel to the surface,

$$\Psi(\mathbf{r})=\psi(y)e^{i\mathbf{k}_\parallel\cdot\mathbf{r}_\parallel}$$

so that $\psi(y)$ satisfies the one-dimensional Schrödinger equation

$$\left[\frac{d^2}{dy^2}+\left[\frac{2m_n}{\hbar^2}(E-V)-k_\parallel^2\right]\right]\psi(y)=0 .$$

We then need to deal only with the perpendicular wave vector q, given by

$$\frac{\hbar^2}{2m_n}(q^2+k_\parallel^2)=(E-V) ,$$

so in the αth region we need only to solve

$$\left[\frac{d^2}{dy^2}+q_\alpha^2\right]\psi(y)=0 \quad \text{for } q_\alpha=\left[\frac{2m_n}{\hbar^2}(E_\perp-V_\alpha)\right]^{1/2} , \tag{2}$$

where q_α and V_α are the perpendicular wave vector and potential energy in the αth region, and $E_\perp=E-\hbar^2k_\parallel^2/2m_n$. (In the rest of this paper we shall choose units so that $\hbar^2/2m_n=1$.) Equation (2) has a general solution $\psi(y)=Ae^{iq_\alpha y}+Be^{-iq_\alpha y}$. However, to determine the constants A and B, we need to fit the boundary conditions, namely, that ψ and $d\psi/dy$ are continuous. It is convenient to solve this using a transfer matrix method.[15] We can write the wave function in the αth region as the sum of a right traveling wave and a left traveling wave

$$\psi_\alpha(y)=a_\alpha e^{iq_\alpha(y-y_\alpha)}+b_\alpha e^{-iq_\alpha(y-y_\alpha)} ,$$

and let us represent $\psi_\alpha(y)$ by a vector $\binom{a_\alpha}{b_\alpha}$ at the interface $y=y_\alpha$. Then, at the first interface $y=y_1=0$, $\psi=\binom{1}{r}$, and at the last interface $y=y_{n-1}$, $\psi=\binom{t}{0}$. These can then be related by a *transfer matrix* $\underline{M}$ as

$$\begin{pmatrix}1\\ r\end{pmatrix}=\begin{pmatrix}M_{11} & M_{12}\\ M_{21} & M_{22}\end{pmatrix}\begin{pmatrix}t\\ 0\end{pmatrix} . \tag{3}$$

The transmission and specular reflection coefficients, t and r, are then given by $t=1/M_{11}$ and $r=M_{21}/M_{11}$. The matrix $\underline{M}$ is given by

$$\underline{M}=\underline{D}^{-1}(q_1)\left[\prod_{j=2}^{N-1}[\underline{D}(q_j)\underline{P}(q_j,d_j)\underline{D}^{-1}(q_j)]\right]\underline{D}(q_N) , \tag{4}$$

where $\{\underline{D}(q_\alpha)\}$ are *transmission matrices* and $\{\underline{P}(q_\alpha,d_\alpha)\}$ are *propagation matrices* for the αth region, and $d_\alpha=y_\alpha-y_{\alpha-1}$ is the width of the αth region. We shall now derive expressions for these matrices. Near the interface between two adjacent regions (call them α and $\alpha+1$) we can write

$$\psi_\alpha=a_\alpha e^{iq_\alpha(y-y_\alpha)}+b_\alpha e^{-iq_\alpha(y-y_\alpha)} \quad \text{for } y_{\alpha-1}<y<y_\alpha ,$$

$$\psi_{\alpha+1}=a_{\alpha+1}e^{iq_{\alpha+1}(y-y_\alpha)}+b_{\alpha+1}e^{-iq_{\alpha+1}(y-y_\alpha)} \quad \text{for } y_\alpha<y<y_{\alpha+1} ,$$

where $y=y_\alpha$ defines the interface. The condition that ψ and $d\psi/dy$ are continuous at $y=y_\alpha$ can be met if

$$a_\alpha+b_\alpha=a_{\alpha+1}+b_{\alpha+1} ,$$

$$q_\alpha(a_\alpha-b_\alpha)=q_{\alpha+1}(a_{\alpha+1}-b_{\alpha+1}) ,$$

which we can rewrite as

$$\underline{D}(q_\alpha)\begin{pmatrix}a_\alpha\\ b_\alpha\end{pmatrix}=\underline{D}(q_{\alpha+1})\begin{pmatrix}a_{\alpha+1}\\ b_{\alpha+1}\end{pmatrix} , \tag{5}$$

where the transmission matrices $\underline{D}(q_\alpha)$ and $\underline{D}(q_{\alpha+1})$ are given by

$$\underline{D}(q_\alpha)=\begin{pmatrix}1 & 1\\ q_\alpha & -q_\alpha\end{pmatrix} . \tag{6}$$

Between the two interfaces bounding the αth region, it is necessary to change the phases of the left and right traveling waves using the propagation matrix

$$\underline{P}(q_\alpha,d_\alpha)=\begin{pmatrix}e^{-iq_\alpha d_\alpha} & 0\\ 0 & e^{iq_\alpha d_\alpha}\end{pmatrix} . \tag{7}$$

Hence the transfer matrix for an n-region system can be written in terms of transmission and propagation matrices as in Eq. (4).

As a simple example, let us calculate the reflectivity of the substrate alone. In this case, we have only two regions, and the transfer matrix $\underline{M}$ is given by

$$\underline{M}=\underline{D}^{-1}(q_1)\underline{D}(q_2)=\frac{1}{2}\begin{pmatrix}1+q_2/q_1 & 1-q_2/q_1\\ 1-q_2/q_1 & 1+q_2/q_1\end{pmatrix} ,$$

and so the reflection and transmission coefficients are $r=M_{21}/M_{11}=(q_1-q_2)/(q_1+q_2)$ and $t=1/M_{11}=2q_1/(q_1+q_2)$, the familiar Fresnel results.

III. SINGLE MAGNETIC LAYER

In this section we consider the simplest example of a single magnetic film on a nonmagnetic substrate. The potential energy in the αth region V_α [in Eq. (2)] can be written as a sum of a nuclear term and a magnetic term

$$V_\alpha=\frac{\hbar^2}{2\pi m_n}\rho_\alpha b_\alpha-\boldsymbol{\mu}_n\cdot\mathbf{B}_\alpha , \tag{8}$$

where $\boldsymbol{\mu}_n$, b_α, $\mathbf{B}_\alpha$, and ρ_α are the neutron moment, coherent nuclear scattering length, magnetic field (due to the magnetization in the region), and atomic density, respectively. This gives rise to a reflectivity that depends on the relative orientation of the spin of the incident neutron and the magnetization of each magnetic layer. Let

us consider the example of a 100-Å-thick Fe film on a Au substrate. In Fig. 1 (lower panel) we show the reflectivities ($R=|r|^2$) for the incident neutron spin parallel (thick solid line) or antiparallel (dashed line) to the Fe film magnetization. We also show the reflectivity for a pure Au substrate (thin line) and the potential energy (inset) for the two configurations. These are plotted against the incident wave vector $q=q_1$, normalized to the critical wave vector q_c (which is equal to $\sqrt{V_3}$ where V_3 is the substrate potential in this three medium system). The quantity q/q_c is known as the *reduced wave vector*. We choose a convention where ↑ (up) means that the neutron spin is parallel to the film magnetization (and hence the neutron moment is antiparallel to the film magnetization). Below the critical wave vector q_c, only evanescent waves occur in the substrate, and all reflectivities are unity. Above the critical wave vector, the reflectivities all decrease from unity. We note that $R_\uparrow \geq R_\downarrow$ because $V_\uparrow > V_\downarrow$, but that the reflectivities are equal to the pure substrate reflectivity at certain values of q/q_c. At these values, which are different for the two different incident spin directions, there are a whole number of wavelengths in the film and the wave field is perfectly matched on to the substrate. (This condition is analogous to the boundary condition for sound waves in an open pipe.) We also note that $R_\uparrow$ ($R_\downarrow$) attains a maximum (minimum) at different values of q/q_c, where there are an odd number of half wavelengths in the film. (This condition is analogous to the boundary condition for sound waves in a pipe with one end closed.) In addition, $R_\downarrow$ can fall to zero if at its minimum, the condition $q_2^2=q_3q_1$ is fulfilled. (This is the same matching condition as for the "blooming of lenses".) We can directly compare $R(q)$ for the two incident spin states of the neutron using a quantity known as the spin asymmetry, S, given by

$$S=\frac{R_\uparrow-R_\downarrow}{R_\uparrow+R_\downarrow} . \tag{9}$$

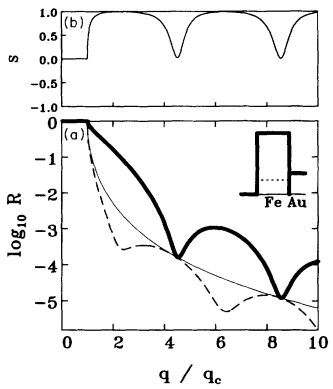

FIG. 1. (a) The reflectivity for up (thick solid line) and down (dashed) incident neutron spin is plotted against reduced wave vector for a (100 Å Fe)/Au film. The reflectivity for a pure Au substrate is also shown (thin solid line). *Inset*: Profile of potential energy through the film for the two spin states. (b) The spin asymmetry $S=(R_\uparrow-R_\downarrow)/(R_\uparrow+R_\downarrow)$ for the same structure.

This is shown in the upper panel of Fig. 1. Since this quantity depends on the thickness and the magnetic moment of the film, measurement of the spin asymmetry can lead to an accurate determination of these quantities. The oscillation period is determined by the thickness, and the magnetic moment determines the amplitude. It is, however, a very weak effect in ultrathin films, and we will describe a method to enhance it in Sec. V.

IV. EXCHANGE BIASED STRUCTURE

In this section we will next discuss a multilayer structure: (20 Å Ag)/(60 Å Fe-Mn)/(40 Å Fe-Ni)/(20 Å

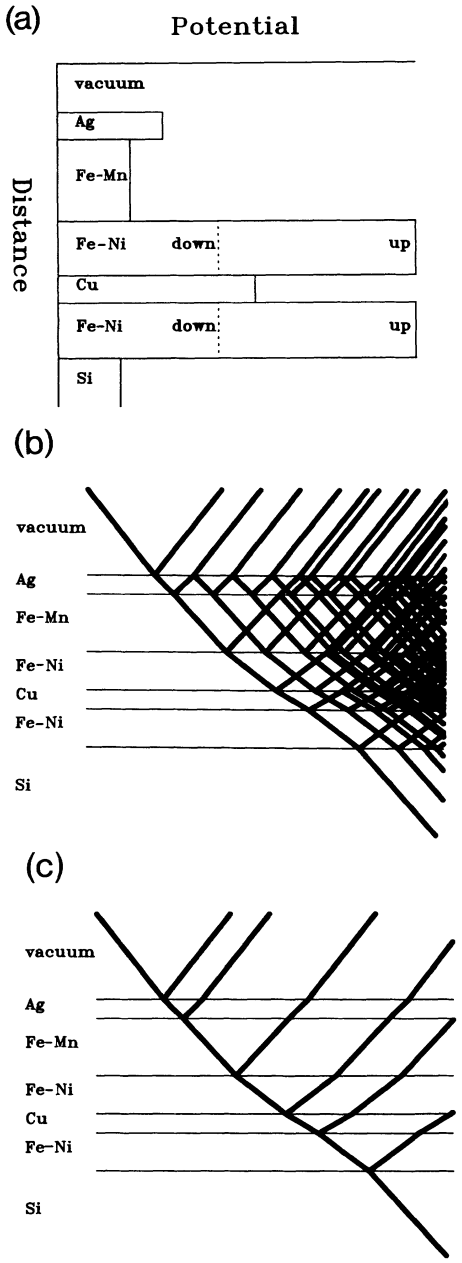

FIG. 2. The exchange-biased structure. (a) The potential energy for the two incident spin states (up=solid, down=dashed). (b) Multiple reflections. (c) Single reflection approximation. (In the experiment, the neutrons approach at glancing incidence.)

Cu)/(40 Å Fe-Ni)/Si. We will defer a full discussion of the reflection from many different orientational configurations in this system until Sec. VII. To begin with we will simply suppose that the magnetic moments in the two Fe-Ni layers are in parallel alignment. This can be readily achieved by the application of an external field (see Sec. VII). Using the matrix method of Sec. II, it is easy to calculate the spin asymmetry resulting from neutron reflection from this structure. However, to obtain greater insight into the processes involved, we will present an important simplification. The neutron potential energy in the film is shown in Fig. 2(a) for the two incident neutron spin states. The neutron reflection for one of these two states is illustrated schematically in Fig. 2(b), clearly showing the abundance of multiple reflections. However, if the incident energy is large with respect to the neutron potential energy anywhere in the film, we imagine that the process of reflection is very weak, and that we need to consider only a single reflection from each layer [Fig. 2(c)]. In this case, the wave vector in the jth region is

$$q_j=\sqrt{q_1^2-V_j}=q_1-\frac{V_j}{2q_1}+O\left[\frac{V_j^2}{q_1^3}\right],$$

if $q_1^2 \gg V_j$. The transmission coefficient between regions j and $j+1$ is given by $t_{j,j+1}=2q_j/(q_j+q_{j+1})=1+O(V/q_j^2)$, and the reflection coefficient is $r_{j,j+1}=(q_j-q_{j+1})/(q_j+q_{j+1})=(V_{j+1}-V_j)/4q_1^2+O(V/q_1^2)$. Hence we can write the total reflectivity of the multilayer to first order as

$$r=\frac{1}{4q_1^2}\sum_{j=1}^{n-1} e^{2iq_1y_j}(V_{j+1}-V_j)\,, \tag{10}$$

which can be rewritten as a Fourier transform of the gradient of the potential energy of the film $r=(4q_1)^{-2}\int e^{2iq_1y}[dV(y)/dy]dy$ since this gradient can be written as a sum of δ functions, one at each interface: $[dV(y)/dy]=\sum_{j=1}^{n-1}(V_{j+1}-V_j)\delta(y-y_j)$. (For the purposes of this paper we will assume perfectly flat interfaces.) In Fig. 3(a), the spin asymmetry calculated using the matrix method in Sec. II is drawn as a thick solid line. The thin solid line shows the contribution from the single reflection [Fig. 2(c)] calculated exactly, without the Fourier transform approximation outlined above. As expected, at large incident wave vectors (larger than about $3q_c$), it agrees extremely well with the matrix calculation, but fails near the critical wave vector, oscillating wildly. The thick solid line is a sum of an infinite series, and so the oscillations in the thin solid line near the critical wave vector can be understood as resulting from the sharp cut-off we have made to this series by only taking the first term. These oscillations die away at higher wave vector when the "one-reflection" approximation we have made becomes a very good one, and the thick and thin solid curves overlap for wave vectors above about $3q_c$. (This value depends on the material parameters.) The Fourier-transform approximation is shown as a dashed line. Here we have taken the "one-reflection" approximation and additionally ignored refraction. This approximation also fails near the critical wave vector, but improves for increasing wave vector, as refraction becomes progressively less important. The approximation does give the correct shape, and can be used to understand the structure in $S(q)$. We conclude that just above the critical wave vector, refraction and multiple reflections dominate the response. At larger wave vectors, the effect can be understood in terms of diffraction alone, since refraction and multiple reflections decrease in importance with increasing wave vector. In Fig. 3(b) the same graphs are plotted for the case in which the moments in the two ferromagnetic layers are in antiparallel alignment, with the moment in the upper Fe-Ni layer rotated by π. (We will discuss how this may be achieved in Sec. VII.) The large difference between the response for the parallel and antiparallel configurations is clearly seen in Fig. 4(a). In Figs. 4(b) and 4(c), we plot the probability density, $|\psi(y)|^2$, for the parallel (FM) and antiparallel (AFM) configurations, respectively, at four values of the wave vector marked in Fig. 4(a) for incident spin up (solid) and spin down (dashed) neutrons. (We stress that the two magnetic layers are only weakly coupled, so that the labels FM and AFM refer to ferromagnetic and antiferromagnetic *alignment*, not coupling.) In both cases, in Figs. 4(b) and 4(c), at wave vector 1, which is below the critical wave vector, only evanescent waves are present in the substrate, and in the vacuum, we see the interference between the incom-

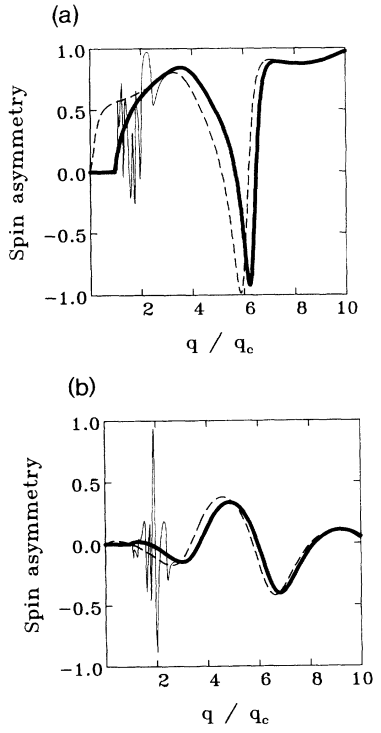

FIG. 3. The spin asymmetry for the (a) FM and (b) AFM aligned exchange-biased structures. The thick solid line shows the exact results, the thin solid line shows the single reflection approximation worked out exactly, and the dashed line shows the Fourier transform approximation of Eq. (10). This thin and thick solid line overlap in both cases for q/q_c greater than about 3, i.e., the single reflection approximation is accurate for this large wave vector range.

ing and reflected waves, resulting in a spatial variation of $|\psi(y)|^2$. Above critical reflection, at wave vectors 2, 3, and 4, traveling waves can propagate in the substrate. We notice that with the antiferromagnetic structure, the two reflectivities for the two different spins are of nearly the same magnitude, but because of the different distribution of potential barriers for the two spin states, there is a difference of phase. In the ferromagnetic case, the up-spin reflectivity is much greater than the down-spin reflectivity, except at the resonance (wave vector 4), where it drops down to a very low value. This is very close to a matching condition, and we notice that there are a whole number of wavelengths fitted into the film. This analysis illustrates the fact that PNR depends upon the complex interference of reflected waves.

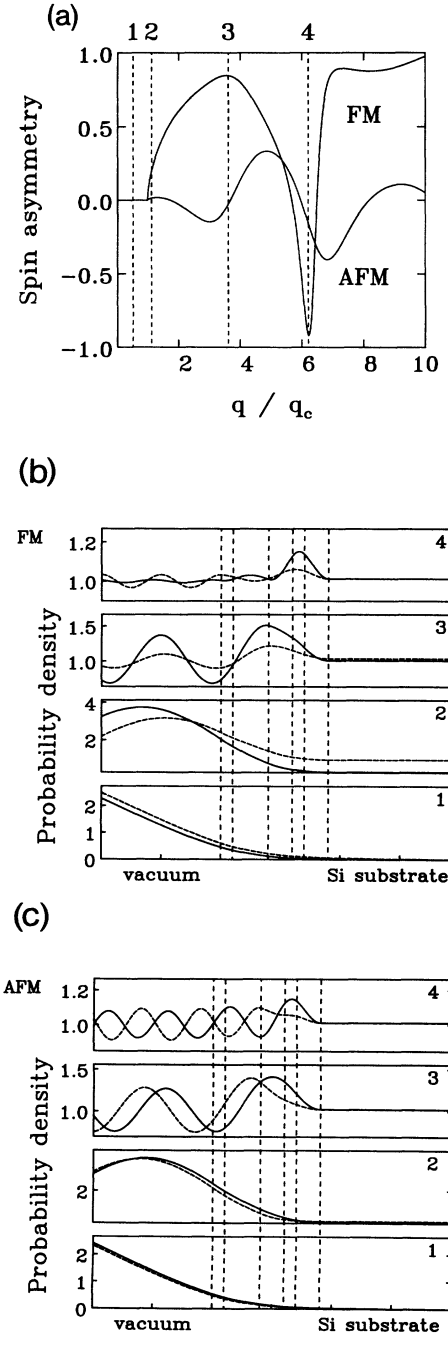

FIG. 4. (a) The spin asymmetry for the FM and AFM aligned exchange-biased structures. The wave field as a function of distance into the film is shown for the (b) FM and (c) AFM cases, at four values of reduced wave vector marked in (a) by vertical dashed lines.

V. OVERLAYER ENHANCEMENT

We have seen that the reflectivity at large wave vector can be quite well approximated by a Fourier transform of the gradient of the potential energy through the film. The single thin layer of Sec. II had two interfaces, and hence the reflectivity at large wave vectors was governed by the Fourier transform of two δ functions, i.e., a sinusoidal function. This in agreement with Fig. 1. For very thin films, the oscillation period is thus very large in reciprocal space. Hence the spin asymmetry can be difficult to detect because the maximum of the oscillation can occur at a value of q much larger than is observable experimentally (in a typical experiment, q is less than about $6q_c$). By evaporating a much thicker nonmagnetic overlayer on top of the magnetic film, it is found that the

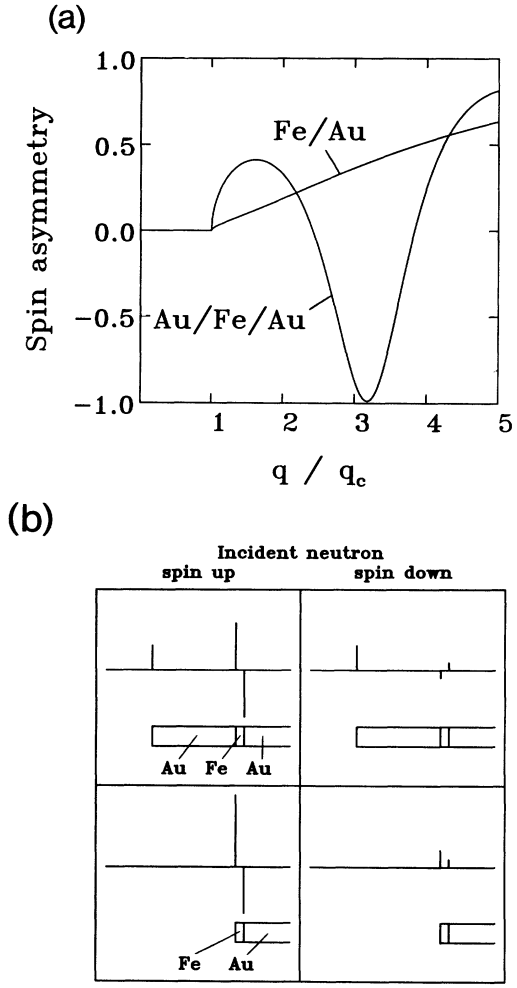

FIG. 5. (a) The spin asymmetry for (10 Å Fe)/Au and (100 Å Au)/(10 Å Fe)/Au. (b) The δ functions of Eq. (10) shown schematically for the two structures, and for incident neutron spin up and down.

spin dependent response is substantially enhanced.[9] We have effectively added a third interface to the system, and hence a third δ function, and this gives an oscillatory component to the reflectivity of a much shorter period. Although the overlayer is nonmagnetic, the total reflectivity depends on all the interfaces since we measure $R=|r|^2$, not r, and hence the magnetic contribution, measured by S, is brought lower in q and is thus easily observable. In Fig. 5(a) we show the spin asymmetry from (10 Å Fe)/Au, and (100 Å Au)/(10 Å Fe)/Au, which illustrates the above argument. The corresponding δ functions are shown in Fig. 5(b). The magnetic effect is similar in both cases, but the effect of the overlayer is to compress the oscillation in q in order to bring the maximum into the experimentally observable range.

VI. SPIN-DEPENDENT NEUTRON REFLECTION

Although we have assumed that the magnetic moment of each region is constant in magnitude and direction throughout that region, it may vary from region to region not only in magnitude, but also in direction. If the direction of the magnetic moment changes between two regions, then so does the axis of quantization, and it is necessary to transform the spinor wave function accordingly. In this paper we will restrict ourselves to changes of moment direction in the plane of the film for simplicity, although other changes can be treated similarly. For example, if the angle of quantization changes from region 1 to region 2 by an angle of θ in the (x,z) plane, then we must replace Eq. (5) with

$$\begin{bmatrix} \underline{D}(q_1^{\uparrow}) & \underline{0} \\ \underline{0} & \underline{D}(q_1^{\downarrow}) \end{bmatrix} \begin{bmatrix} \psi_1^{\uparrow} \\ \psi_1^{\downarrow} \end{bmatrix} = \begin{bmatrix} \cos\left[\frac{\theta}{2}\right]\underline{I} & \sin\left[\frac{\theta}{2}\right]\underline{I} \\ -\sin\left[\frac{\theta}{2}\right]\underline{I} & \cos\left[\frac{\theta}{2}\right]\underline{I} \end{bmatrix} \begin{bmatrix} \underline{D}(q_2^{\uparrow}) & \underline{0} \\ \underline{0} & \underline{D}(q_2^{\downarrow}) \end{bmatrix} \begin{bmatrix} \psi_2^{\uparrow} \\ \psi_2^{\downarrow} \end{bmatrix}, \tag{11}$$

where $\psi_\alpha^s=\begin{pmatrix} a_\alpha^s \\ b_\alpha^s \end{pmatrix}$ is the left and right traveling waves of spin $s=\uparrow,\downarrow$ in region $\alpha=1,2$, and $\underline{I}=\begin{pmatrix} 1 & 0 \\ 0 & 1 \end{pmatrix}$. [Note that each component of the matrices in Eq. (11) above is itself a 2×2 matrix.] We can therefore generalize Eq. (4) and write a 4×4 transfer matrix for the spin dependent potential in Eq. (8):

$$\underline{M}=\underline{D}^{-1}(q_1,q_1)\underline{R}(\theta_{1,2})\left[\prod_{j=2}^{N-1}[\underline{D}(q_j^{\uparrow},q_j^{\downarrow})\underline{P}(q_j^{\uparrow},q_j^{\downarrow},d_j)\underline{D}^{-1}(q_j^{\uparrow},q_j^{\downarrow})\underline{R}(\theta_{j,j+1})]\right]\underline{D}(q_N,q_N), \tag{12}$$

where

$$\underline{D}(q_j^{\uparrow},q_j^{\downarrow})=\begin{bmatrix} \underline{D}(q_j^{\uparrow}) & \underline{0} \\ \underline{0} & \underline{D}(q_j^{\downarrow}) \end{bmatrix}, \tag{13}$$

is the 4×4 generalization of the *transmission matrices*,

$$\underline{P}(q_j^{\uparrow},q_j^{\downarrow},d_j)=\begin{bmatrix} \underline{P}(q_j^{\uparrow},d_j) & \underline{0} \\ \underline{0} & \underline{P}(q_j^{\downarrow},d_j) \end{bmatrix}, \tag{14}$$

is the 4×4 generalization of the *propagation matrices*, and

$$\underline{R}(\theta_{j,j+1})=\begin{bmatrix} \cos(\theta_{j,j+1}/2)\underline{I} & \sin(\theta_{j,j+1}/2)\underline{I} \\ -\sin(\theta_{j,j+1}/2)\underline{I} & \cos(\theta_{j,j+1}/2)\underline{I} \end{bmatrix}, \tag{15}$$

are the matrices for rotating the quantization axis by $\theta_{j,j+1}$ at the j-$(j+1)$ interface.

For incident spin-up neutrons, we may in general write

$$\begin{bmatrix} 1 \\ r_u^{\uparrow} \\ 0 \\ r_u^{\downarrow} \end{bmatrix} = \begin{bmatrix} M_{11} & M_{12} & M_{13} & M_{14} \\ M_{21} & M_{22} & M_{23} & M_{24} \\ M_{31} & M_{32} & M_{33} & M_{34} \\ M_{41} & M_{42} & M_{43} & M_{44} \end{bmatrix} \begin{bmatrix} t_u^{\uparrow} \\ 0 \\ t_u^{\downarrow} \\ 0 \end{bmatrix},$$

by analogy with Eq. (3), from which it is easy to show that

$$t_u^{\uparrow}=M_{33}/(M_{11}M_{33}-M_{13}M_{31}),$$
$$t_u^{\downarrow}=-M_{31}/(M_{11}M_{33}-M_{13}M_{31}),$$
$$r_u^{\uparrow}=(M_{21}M_{33}-M_{23}M_{31})/(M_{11}M_{33}-M_{13}M_{31}),$$
$$r_u^{\downarrow}=(M_{41}M_{33}-M_{43}M_{31})/(M_{11}M_{33}-M_{13}M_{31}),$$

where the subscript u refers to incident spin up, and the superscript refers to the spin state of the transmitted or reflected beam. Similarly, for incident spin-down neutrons

$$\begin{bmatrix} 0 \\ r_d^{\uparrow} \\ 1 \\ r_d^{\downarrow} \end{bmatrix} = \begin{bmatrix} M_{11} & M_{12} & M_{13} & M_{14} \\ M_{21} & M_{22} & M_{23} & M_{24} \\ M_{31} & M_{32} & M_{33} & M_{34} \\ M_{41} & M_{42} & M_{43} & M_{44} \end{bmatrix} \begin{bmatrix} t_d^{\uparrow} \\ 0 \\ t_d^{\downarrow} \\ 0 \end{bmatrix},$$

$$t_d^{\uparrow}=-M_{13}/(M_{11}M_{33}-M_{13}M_{31}),$$
$$t_d^{\downarrow}=M_{11}/(M_{11}M_{33}-M_{13}M_{31}),$$
$$r_d^{\uparrow}=(M_{23}M_{11}-M_{21}M_{13})/(M_{11}M_{33}-M_{13}M_{31}),$$
$$r_d^{\downarrow}=(M_{43}M_{11}-M_{41}M_{13})/(M_{11}M_{33}-M_{13}M_{31}),$$

where the subscript d refers to incident spin down. The spin asymmetry, Eq. (9), can now be written

$$S=\frac{|r_u^{\uparrow}|^2+|r_u^{\downarrow}|^2-|r_d^{\uparrow}|^2-|r_d^{\downarrow}|^2}{|r_u^{\uparrow}|^2+|r_u^{\downarrow}|^2+|r_d^{\uparrow}|^2+|r_d^{\downarrow}|^2} . \tag{16}$$

Hence the spin asymmetry is in general a function of four reflection processes, resulting from the possibility of a spin-flip reflection. We may now calculate the spin asymmetry in multilayers whose coupling is more complicated than simple ferromagnetic or antiferromagnetic. However, before giving an example, it is useful to have a more intuitive picture of the reflection process, analogous to the Fourier transform result of Sec. IV. Consider a beam of spin-up neutrons of unit amplitude approaching the interface between two regions [Fig. 6(a)]. Using the formalism above, it is easy to show that the transmission and reflection coefficients through the interface are given by

$$t_{\uparrow}=\frac{2q_1^{\uparrow}(q_1^{\downarrow}+q_2^{\downarrow})\cos(\theta_2/2)}{\cos^2(\theta_2/2)(q_1^{\uparrow}+q_2^{\uparrow})(q_1^{\downarrow}+q_2^{\downarrow})+\sin^2(\theta_2/2)(q_1^{\uparrow}+q_2^{\downarrow})(q_1^{\downarrow}+q_2^{\uparrow})} ,$$

$$t_{\downarrow}=\frac{2q_1^{\uparrow}(q_1^{\downarrow}+q_2^{\uparrow})\sin(\theta_2/2)}{\cos^2(\theta_2/2)(q_1^{\uparrow}+q_2^{\uparrow})(q_1^{\downarrow}+q_2^{\downarrow})+\sin^2(\theta_2/2)(q_1^{\uparrow}+q_2^{\downarrow})(q_1^{\downarrow}+q_2^{\uparrow})} ,$$

$$r_{\uparrow}=\frac{\cos^2(\theta_2/2)(q_1^{\uparrow}-q_2^{\uparrow})(q_1^{\downarrow}+q_2^{\downarrow})+\sin^2(\theta_2/2)(q_1^{\uparrow}-q_2^{\downarrow})(q_1^{\downarrow}+q_2^{\uparrow})}{\cos^2(\theta_2/2)(q_1^{\uparrow}+q_2^{\uparrow})(q_1^{\downarrow}+q_2^{\downarrow})+\sin^2(\theta_2/2)(q_1^{\uparrow}+q_2^{\downarrow})(q_1^{\downarrow}+q_2^{\uparrow})} ,$$

$$r_{\downarrow}=\frac{2q_1^{\uparrow}\cos(\theta_2/2)\sin^2(\theta_2/2)(q_2^{\uparrow}-q_2^{\downarrow})}{\cos^2(\theta_2/2)(q_1^{\uparrow}+q_2^{\uparrow})(q_1^{\downarrow}+q_2^{\downarrow})+\sin^2(\theta_2/2)(q_1^{\uparrow}+q_2^{\downarrow})(q_1^{\downarrow}+q_2^{\uparrow})} ,$$

where θ_2 is the angle between the quantization axis (i.e., magnetic moment) in the second region, and the quantization axis of the incident neutrons in the vacuum. Hence, in the large incident energy limit, $q_1^2=q_1^{\uparrow 2}\gg\max(V_1^{\uparrow},V_1^{\downarrow},V_2^{\uparrow},V_2^{\downarrow})$, we have

$$\begin{aligned}
t_{\uparrow}&=\cos\left[\frac{\theta_2}{2}\right]+O\left[\frac{V}{q_1^2}\right] ,\\
t_{\downarrow}&=\sin\left[\frac{\theta_2}{2}\right]+O\left[\frac{V}{q_1^2}\right] ,\\
r_{\uparrow}&=\frac{1}{4q_1^2}\left[\cos^2\left[\frac{\theta_2}{2}\right](V_2^{\uparrow}-V_1^{\uparrow})\right.\\
&\qquad\left.+\sin^2\left[\frac{\theta_2}{2}\right](V_2^{\downarrow}-V_1^{\uparrow})\right]+O\left[\frac{V^2}{q_1^4}\right] ,\\
r_{\downarrow}&=\frac{1}{4q_1^2}\cos\left[\frac{\theta_2}{2}\right]\sin\left[\frac{\theta_2}{2}\right](V_2^{\downarrow}-V_2^{\uparrow})+O\left[\frac{V^2}{q_1^4}\right] .
\end{aligned} \tag{17}$$

In a multilayer [Fig. 6(b)], each interface will give a contribution to the total reflectivity and in the high energy limit, these contributions can simply be summed, since multiple reflections can be ignored. It is important, however, to be careful to rotate all components back into the frame of reference of the first region. After some manipulations, this yields

$$\begin{aligned}
r_{\uparrow}&=\frac{1}{4q_1^2}\sum_{j=1}^{n-1}e^{2iqy_j}\sum_{\sigma=\pm 1}\frac{1}{2}[\,V_{j+1}^{\sigma}(1+\sigma\cos\theta_{j+1})\\
&\qquad -V_j^{\sigma}(1+\sigma\cos\theta_j)] ,\\
r_{\downarrow}&=\frac{1}{4q_1^2}\sum_{j=1}^{n-1}e^{2iqy_j}\sum_{\sigma=\pm 1}\frac{\sigma}{2}(V_j^{\sigma}\sin\theta_j-V_{j+1}^{\sigma}\sin\theta_{j+1}) ,
\end{aligned} \tag{18}$$

where the spin index σ is $+1$ (-1) for $\uparrow$ $(\downarrow)$ spin, and where θ_j is the angle between the quantization axis (i.e., magnetic moment) in the jth region, and the quantization axis of the incident neutrons in the vacuum. This has all been derived for an incident neutron beam which is spin up. A corresponding expression can be derived for incident spin down and the spin asymmetry, S, can be calculated using Eq. (16).

VII. SENSITIVITY TO CONFIGURATION

We now return to the exchange-biased structure considered in Sec. IV. In small fields the Fe-Ni layer adjacent to the Fe-Mn is pinned by the unidirectional exchange anisotropy and so the direction of its magnetic moment is fixed and independent of the direction of the applied field. The other, uncoupled, soft Fe-Ni layer can be saturated in the plane with a very small field, and is thus free to rotate in the plane as this applied field rotates, for appropriate values of the applied magnetic field.[8] In this way, the vector magnetization of the two layers can be varied in a controllable manner, and we illustrate our discussion of the PNR technique by considering the corresponding response in $S(q)$.

The experimental arrangement is shown schematically in Fig. 7(a). The sample is held in an in-plane applied magnetic field (whose direction serves as the quantization axis for the neutrons in the vacuum), and the moment in the free Fe-Ni layer ($\mathbf{M}_2$ in the figure) becomes immediately aligned with the field. We can vary the direction of the moment of the other Fe-Ni layer ($\mathbf{M}_1$) in two ways. First, by keeping the applied field well below the unidirectional anisotropy field, $\mathbf{M}_1$ remains pinned by the Fe-Mn layer, and so its direction can be rotated in-plane by rotating the entire sample about an axis normal to the surface. Second, the sample can be mounted so that the direction of unidirectional anisotropy is in-plane but at

right angles to the applied field, and the spin dependent reflectivity is then studied as a function of applied field. Using a simple energy argument, we would expect this magnetization change to occur by single domain rotation. Experimentally, the second method is preferred, since the first could be complicated by possible problems of sample misalignment, inherent in the need to rotate the sample. It should be noted that the second method allows θ to vary between 0 and $\pi/2$ only (whereas the first allows any angle) so that the $3\pi/4$ and π simulations below could not be realized experimentally by the second method.

In Fig. 7(b) we show the calculated spin asymmetry for this structure as we rotate the pinned Fe-Ni layer in the plane around from pure parallel to pure antiparallel alignment. We first notice that the change in direction of the moment of this Fe-Ni layer produces a marked

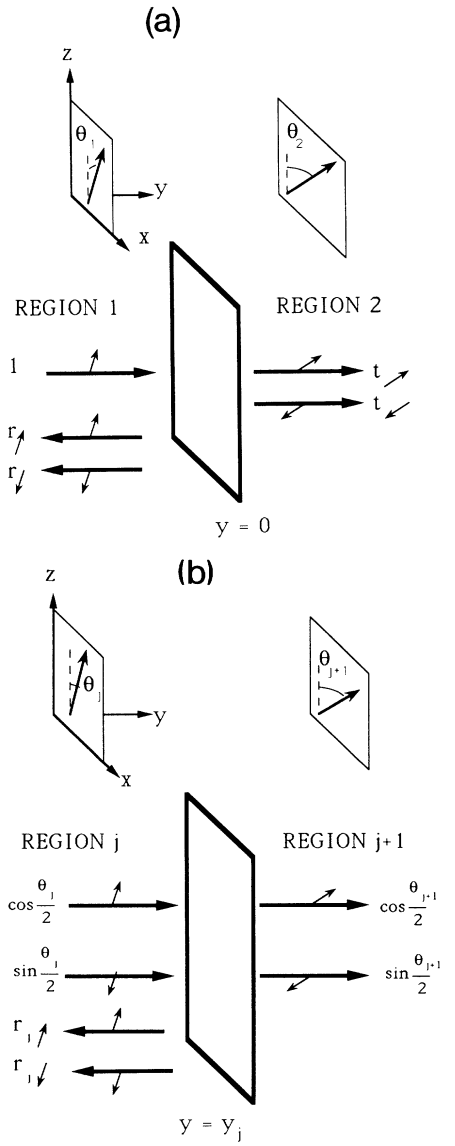

FIG. 6. (a) The interface between two magnetic regions (regions 1 and 2), showing the different quantization axes in the plane for the two regions. (b) Part of an n-layer multilayer, at the j-$(j+1)$ layer interface.

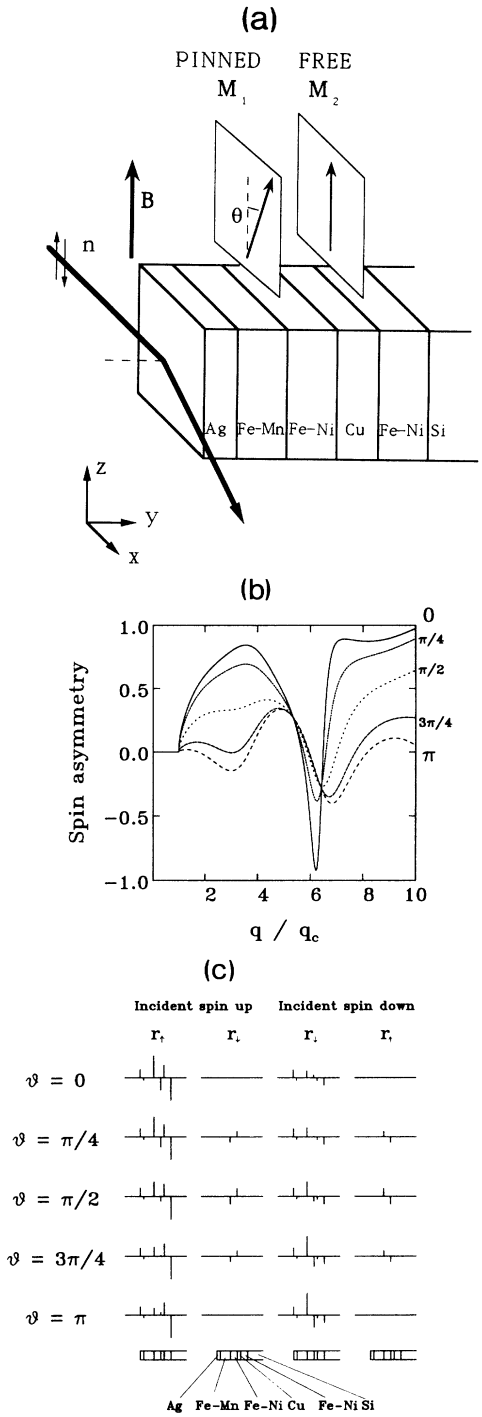

FIG. 7. (a) The PNR experiment on an exchange-biased structure shown schematically. The up- and down-spin directions of the incident neutron n are determined by the direction of the applied field **B**. The moment in the free Fe-Ni layer ($\mathbf{M}_2$) is aligned with the field. The moment in the pinned Fe-Ni layer adjacent to the Fe-Mn layer ($\mathbf{M}_1$) is at an angle θ to the applied field (see text). Both $\mathbf{M}_1$ and $\mathbf{M}_2$ are in the plane of the film. (b) The spin asymmetry for the spin valve structure for five different orientations of the moment in the free Fe-Ni layer. The angles 0, $\pi/4$, $\pi/2$, $3\pi/4$, and π are measured with respect to the exchange biased Fe-Ni layer. (c) The δ functions of Eq. (18) shown for these five angles, and for reflected spin-up and -down neutrons from incident spin-up and spin-down neutrons.

change in the spin asymmetry which is easily detected experimentally. Using the approximation of Eq. (18), the up and down reflectivities are simply the Fourier transforms of $n-1$ δ functions located at the interfaces with amplitudes at the jth interface of $(4q_1)^{-2}\sum_{\sigma=\pm1}\frac{1}{2}[V^{\sigma}_{j+1}(1+\sigma\cos\theta_{j+1})-V^{\sigma}_{j}(1+\sigma\cos\theta_j)]$ and $(4q_1^2)^{-2}\sum_{\sigma=\pm1}(\sigma/2)(V^{\sigma}_{j}\sin\theta_j-V^{\sigma}_{j+1}\sin\theta_{j+1})$ for up and down spins, respectively. These amplitudes are shown in Fig. 7(c) for the cases of incident up and down spin and for each of the five configurations shown in Fig. 7(b). The angle between the moment of the two Fe-Ni layers is denoted by θ. We notice that spin-flip reflection is not observed for $\theta=0$ or π. This is because it is only when there is some component of the magnetic moment in the film which is perpendicular to the incident neutron spin, that Larmor precession of the neutron spin can occur. Also, we notice that the spin asymmetry, S, calculated in Eq. (16), is the result a combination of the modulus square of four sets of Fourier transforms, one from each column of the schematic table in Fig. 7(c). We stress that these results only apply to the case in which the ferromagnetic layers are single domain. If they are not, it is necessary to perform some "average over configurations," although it is normally not clear how this average should be taken, unless independent information about the domain distribution is available. However, it is clear from this simulation that changes in the relative orientation of the ferromagnetic moments produces large and easily measurable changes in the spin-dependent reflectivity.

In this paper we have calculated the spin-dependent reflectivity assuming certain specified magnetic configurations. The experimental situation requires an analysis which is the reverse of this process: given a measured spin asymmetry $S(q)$, can we deduce the magnetization-vector profile, $\mathbf{M}(y)$? For a structure in which each magnetic layer is single domain, our calculations suggest that this is possible. We have demonstrated that measurably different $S(q)$ result for each magnetic orientation, although certain symmetry related configurations do produce identical $S(q)$ behavior. Therefore, by comparing the results of experiment with simulations, the magnetization vector in each layer can be determined provided these vector magnetizations are the only unknown variables. The appropriate experimental procedure is as follows: $S(q)$ should be initially measured for a given sample in an in-plane applied field greater than the saturation field. With the moment in each layer thus aligned, it is then possible to adjust the estimates of the values of layer thicknesses, layer densities, and layer moments to obtain the best fit to the measured $S(q)$. In subsequent measurements at lower applied fields, the moments in each layer will no longer be necessarily aligned, leading to different $S(q)$ behavior. The only remaining adjustable parameters in fitting this data are the directions of the magnetic moments in each layer, and by comparing $S(q)$ calculated for a range of angular orientations θ_i, $S(q)$ can be fitted. For a system with a large number of magnetic layers, this procedure will be computationally demanding, but nonetheless possible. However, the technique is ideally suited to studying the coupling in bilayer systems. In the case in which each ferromagnetic layer breaks up into domains, the neutron reflectivity will be much more complicated in general, and PNR measurements are insufficient to determine the spatially varying magnetization structure. Appropriate averaging procedures, depending on whether the coherence length of the neutrons are larger or smaller than the domain size, will however allow some estimate of the spatially averaged vector magnetization within each layer. Nonetheless, PNR measurements can be extremely valuable in providing an assessment of how closely such a system approximates to single domain behavior. Furthermore, in contrast to surface sensitive techniques, PNR can be used to probe embedded layers.

VIII. CONCLUSION

We have shown how the magnetic moment of thin films and the magnetization-vector profile of multilayers can be measured using polarized neutron reflection. A transfer matrix method has been described for calculating spin dependent neutron reflectivities. The form of the spin asymmetry is dominated by multiple reflections and refraction just above the critical wave vector, but with increasing wave vector, such processes become progressively less important, and the response moves toward a "diffraction limit" in which a Fourier transform approximation to the exact result can be used. PNR is a sensitive probe of the orientation of magnetizations in magnetic multilayers and therefore can be used to study the magnetization reversal process in detail.

ACKNOWLEDGMENTS

We are grateful to the United Kingdom Science and Engineering Research Council for financial support and to Dr. V. Speriosu for valuable discussions.

[1]P. Grünberg, R. Schreiber, Y. Pang, M. N. Brodsky, and H. Sowers, Phys. Rev. Lett. **57**, 2442 (1986).

[2]C. Carbone and S. F. Alvorado, Phys. Rev. B **36**, 2433 (1987).

[3]J. Kwo, M. Hong, F. J. DiSalvo, J. V. Waszxzak, and C. F. Majkrzak, Phys. Rev. B **35**, 7295 (1987).

[4]D. Pescia, D. Kerkmann, F. Schumann, and W. Gudat, Z. Phys. B **78**, 475 (1990); S. S. P. Parkin, R. Bhadra, and K. P. Roche, Phys. Rev. Lett. **66**, 2152 (1991).

[5]S. S. P. Parkin, N. More, and K. P. Roche, Phys. Rev. Lett. **64**, 2304 (1990).

[6]D. M. Edwards and J. Mathon, J. Magn. Magn. Mater. **93**, 85 (1991); D. M. Edwards, J. Mathon, R. B. Muniz, and M. S. Phan, Phys. Rev. Lett. **67**, 493 (1991).

[7]M. N. Baibich, J. M. Broto, A. Fert, F. Nguyen van Dau, F. Petroff, P. Etienne, G. Creuzet, A. Friederich, and J. Chazelas, Phys. Rev. Lett. **61**, 2472 (1988).

[8]B. Dieny, V. S. Speriosu, S. S. Parkin, B. A. Gurney, D. R. Wilhoit, and D. Mauri, Phys. Rev. B **43**, 1297 (1991).

[9]J. A. C. Bland, D. Pescia, and R. F. Willis, Phys. Rev. Lett. **58**, 1244 (1987); D. Pescia, R. F. Willis, and J. A. C. Bland, Surf.

Sci. **189**, 724 (1987).
[10]J. A. C. Bland, R. D. Bateson, A. D. Johnson, B. Heinrich, Z. Celinski, and H. J. Lauter, J. Magn. Magn. Mater. **93**, 331 (1991).
[11]J. A. C. Bland, R. D. Bateson, P. C. Riedi, R. G. Graham, H. J. Lauter, C. Shackleton, and J. Penfold, J. Appl. Phys. **69**, 4989 (1991).
[12]J. A. C. Bland, A. D. Johnson, H. J. Lauter, R. D. Bateson, S. J. Blundell, C. Shackleton, and J. Penfold, J. Magn. Magn. Mater. **93**, 513 (1991).
[13]S. S. P. Parkin, V. R. Deline, R. O. Hilleke, and G. P. Felcher, Phys. Rev. B **42**, 10 583 (1990).
[14]J. A. C. Bland and R. F. Willis, in *Thin Film Growth Techniques for Low Dimensional Structures,* edited by R. F. C. Farrow, S. S. P. Parkin, P. J. Dobson, J. H. Neave, and A. S. Arrott (Plenum, New York, 1987).
[15]P. Yeh, *Optical Waves in Layered Media* (Wiley, New York, 1988).